Computational Analysis of Lithium Ion Battery Cathode Performance

Hussein Subhi Al-Rikabi[1], Nour Abdalrazaq Hassan[1], Widad Hano Albanda[2], Esmaeil Jalali Lavasani[3] and Muhammad Hameed Al-Timimi[1]

[1]*Department of Physics, College of Science, University of Diyala, 32001 Baqubah, Diyala, Iraq*

[2]*Department of Science, College of Basic Education, Mustansiriyah University, 10052 Baghdad, Iraq*

[3]*Nano-SAE Research Center, Faculty of Physics, University of Bucharest, Atomistilor Str. 405, 077125 Măgurele, Romania*

hussein.s.al.rikabi@gmail.com, {noor, muhammadtimimi}@uodiyala.edu.iq, wadad.hanu@uomustansiriyah.edu.iq, esmaeil.jalali@3nanosae.org

Keywords: Lithium-Ion Batteries, Urea Route, Nanomaterials, LMO, LMNO, Cathode Materials.

Abstract: This study reports on the preparation and investigation of the structural and morphological properties, as well as the electrochemical behavior, of the nanostructured cathode materials $LiMn_2O_4$ and $Li_{1.2}Mn_{1.6}Ni_{0.2}O_4$ synthesized via a urea-assisted route. A two-step heat treatment (450 °C for 4 h followed by 800 °C for 5 h) led to the formation of a highly crystalline, single-phase spinel, as confirmed by X-ray diffraction (XRD) patterns, with a contraction of the lattice parameter from (8.32 to 8.19) Å and a decrease in the average crystallite size from (30.14 to 28.94) nm upon nickel incorporation and lithium enrichment in the structure. Field-emission scanning electron microscopy (FE-SEM) images revealed homogeneous octahedral particles, with the average particle size decreasing from (1.15 to 0.44) μm for the doped sample, confirming the effectiveness of the urea route in tailoring the microstructure. Electrochemically, the $Li_{1.2}Mn_{1.6}Ni_{0.2}O_4$ electrode delivered an initial charge/discharge capacity of (245.82/230.51) $mAh.g^{-1}$ and a coulombic efficiency of (93.77%), outperforming $LiMn_2O_4$ (213.45/192.80 $mAh.g^{-1}$, 90.32% efficiency), together with a marked decrease in charge-transfer resistance and an enhancement in capacity retention to (90.28%) after 100 cycles compared with (86.10%) for the undoped composition. These results demonstrate that the nanostructured spinel $Li_{1.2}Mn_{1.6}Ni_{0.2}O_4$ prepared via the urea route operates efficiently as a cathode in high-voltage lithium-ion batteries fabricated and tested in this study.

1 INTRODUCTION

There are numerous studies on lithium-ion batteries and related materials to provide new and improved energy sources for portable gadgets such as computers and mobile phones. In addition, to reduce risks to the environment, energy storage systems are currently receiving significant attention, especially in applications such as cars and stationary vehicles [1]-[5]. Among the many advantages to consider are low cost and abundance, so transition metal oxides such as $LiMn_2O_4$ and $LiMnO_2$ are often studied [6], [7]. In addition to these advantages, manganese ions have more than one oxidation state, and multiple and unique forms of manganese oxide can be obtained [8]. $LiMnO_2$ resembles the layered phase (R-3m) of $LiCoO_2$, but this phase is thermally unstable, transforming into the more stable cubic spinel phase (Fd-3m) during calcination at high temperatures or during charging and discharging. This transformation is associated with the presence of the Mn^+ ion, which undergoes a Jahn–Teller distortion, resulting in distortion of the crystal lattice and a decrease in performance [9]. Therefore, nanomaterials made from $LiMn_2O_4$ are of great fundamental and technological importance in the cathode of rechargeable lithium-ion batteries. Numerous studies have concentrated about spinel compounds replaced with transition metals, exemplified as $LiM_xMn_{2-x}O_4$ (where M = Cr, Co, Fe, Ni, Cu) [6]. Lazarraga et al. synthesized a nanosized $LiNi_{0.5}Mn_{1.5}O_4$ spinel using a sucrose-assisted combustion technique [10]. Shaju and Bruce synthesized nano-$LiNi_{0.5}Mn_{1.5}O_4$ synthesized by a resorcinol-formaldehyde-assisted solution method, organized and disordered spinels at 700°C and 750°C,

respectively [11]. The lithium manganese nickel LMN cathode materials are interesting candidates for cathodes owing to their elevated discharge capacity exceeding 200 mAh g^{-1} and energy density surpassing 800 Wh kg^{-1} [12], [13]. This study aims to prepare and fabricate cathodes for lithium-ion batteries based on $LiMn_2O_4$ and $Li_{1.2}Mn_{1.6}Ni_{0.2}O_4$ using the urea combustion route, and to elucidate the effect of lithium enrichment and nickel doping in the spinel phase on enhancing the structural and electrochemical properties of the prepared cathodes, by analyzing their crystal structure using X-ray diffraction (XRD), examining the surface morphology and elemental distribution by field-emission scanning electron microscopy (FE-SEM) and energy-dispersive X-ray spectroscopy (EDS), as well as evaluating the electrochemical performance of the assembled lithium-ion batteries through cyclic voltammetry (CV), electrochemical impedance spectroscopy (EIS), and galvanostatic charge–discharge tests and stability over repeated cycling.

2 EXPERIMENTAL PROCEDURES

$LiMn_2O_4$ and $Li_{1.2}Mn_{1.6}Ni_{0.2}O_4$ samples were prepared using the urea route method. Equivalent amounts of lithium chloride (LiCl, 98% purity) and manganese (II) chloride tetrahydrate ($MnCl_2.4H_2O$, 98% purity) were dissolved separately in deionized water, and the two solutions were placed on a magnetic stirrer without heating. Then, citric acid ($C_6H_8O_7$, 99% purity) was dissolved in a molar ratio of 2:1 (citric acid to total metals) in deionized water. The solutions were placed on a magnetic stirrer without heating, and drop by drop, the citric acid solution was added to the (LiCl + $MnCl_2{\cdot}4H_2O$) solution to make a total of 100 mL. Urea (98% purity, NH_2, CO_2, NH_2) was added at urea to total metals in a molar ratio of 1:1, followed by nitric acid (98% purity, HNO_3) at a volume ratio of 0.1:1 (nitric acid to total solution) dropwise. The solution temperature was raised to 80-90°C. After a period of time, the solution formed a gel. With that, it was dried for four hours at 180°C. The sample was then finely ground. The resulting powder was calcined in two stages: the first at 450°C for 4 h in air and the second at 800°C for 5 h in air at a heating rate of 7°C/min. The resulting powder was ground to obtain the final powder. For the $Li_{1.2}Mn_{1.6}Ni_{0.2}O_4$ sample, nickel (II) chloride hexahydrate (98% purity, $NiCl_2.6H_2O$), $MnCl_2.4H_2O$, and LiCl were dissolved in molar ratios of (0.1:0.8:1.1), respectively, in deionized water. The same procedures were followed for the previous sample to obtain the final powder. The prepared samples were examined using XRD (Aeris Research Edition Benchtop X-ray Diffractometer) utilizing Cu Kα radiation (λ=1.5406 Å) at a 2θ angle ranging from 10 to 80 °C to confirm their crystal structure. The distribution and morphology of the elements were examined utilizing a Tescan Mira3 FESEM with an adjustable accelerating voltage (0.2 to 1 kV) and a terminal current of 2 pA. Figure 1 Schematic diagram of the urea route for the prepared nanopowders.

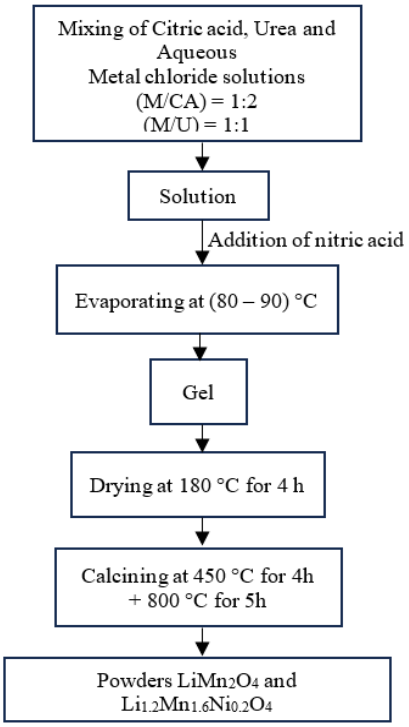

Figure 1: Schematic diagram of the urea route for preparing $LiMn_2O_4$ and $Li_{1.2}Mn_{1.6}Ni_{0.2}O_4$ nanopowders.

Coin-type lithium-ion cells were fabricated using a (1 M) solution of lithium perchlorate ($LiClO_4$) in propylene carbonate as the electrolyte. Cathode electrodes were prepared from the synthesized active materials with the addition of graphite and a PVDF binder; the resulting slurry was coated onto aluminum foil current collectors, dried, and pressed to obtain mechanically stable electrodes. Metallic lithium was used as the anode, and a porous polypropylene (Celgard) membrane pre-soaked in the electrolyte served as the separator between the two electrodes. All cell components were assembled in an argon-filled glove box to minimize exposure to moisture and oxygen. The fabricated cells were subjected to

electrochemical measurements, including cyclic voltammetry (CV), electrochemical impedance spectroscopy (EIS), and galvanostatic charge–discharge tests, in order to evaluate their performance and cycling stability.

3 RESULTS AND DISCUSSION

3.1 XRD Pattern

Figure 2(A1) shows the X-ray diffraction (XRD) pattern of the $LiMn_2O_4$ sample; clear, distinct, and highly crystalline peaks of the cubic spinel phase appear at angles 18.41, 36.01, 37.67, 43.85, 48.06, 58.17, 63.94, 67.25, and 76.86 and have Miller indices of (111), (311), (222), (400), (331), (511), (440), (531), and (622), respectively, within the Fd-3m space group, which matches the standard pattern ICSD 01-088-1749. The lattice constant of sample A1 was calculated to be 8.32 Å, which is close to the standard value of 8.24 Å. Figure 2(A2) The XRD pattern of the $Li_{1.2}Mn_{1.6}Ni_{0.2}O_2$ sample shown a slight shift in the peak positions to the right. This shift is attributed to the replacement of Mn^{3+} ions with a larger ionic radius (0.65 Å) by Ni^{3+} ions with a smaller ionic radius (0.60 Å), which leads to lattice shrinkage. The lattice constant of sample A2 (8.19 Å) was lower than that of sample A1 [14]. Using Scherrer's equation, the crystallite size was calculated, which showed a slight decrease from 30.14 nm to 28.94 nm. The lattice strain for both samples was 0.003, which indicates high crystal stability, and the nickel introduction process did not significantly affect the crystal structure [15]-[18], Table 1 shows some crystal parameters A1) $LiMn_2O_4$. A2) $Li_{1.2}Mn_{1.6}Ni_{0.2}O_4$.

3.2 FE-SEM and EDS

Morphology and particle size distribution of the produced samples were analyzed using a field-emission scanning electron microscope (FESEM). The FESEM images in Figures 3 and 4 show that samples A1 and A2 have octahedral structures, indicating sufficient crystal growth during the calcination process without obvious agglomeration, demonstrating the homogeneity and stability of the structures produced by the urea route preparation method. The uniform octahedral enhances the electrochemical efficacy of cathode materials by reducing the grain boundary resistance, facilitating lithium-ion transport during charging and discharging, and maintaining a stable crystal structure. The particle size distribution in Figure 5 shows a decrease in the average particle size upon the addition of nickel from 1.15 µm to 0.44 µm, which is consistent with the X-ray diffraction (XRD) results [19]-[21]. Energy dispersive spectroscopy (EDS) analysis in Figure 6 confirmed the presence of the elements O, Mn, and Ni in weight and atomic ratios as shown in Table 2, which are close to theoretical values, noting that the lithium element is not present due to the limitations of the EDS technique [22], [23].

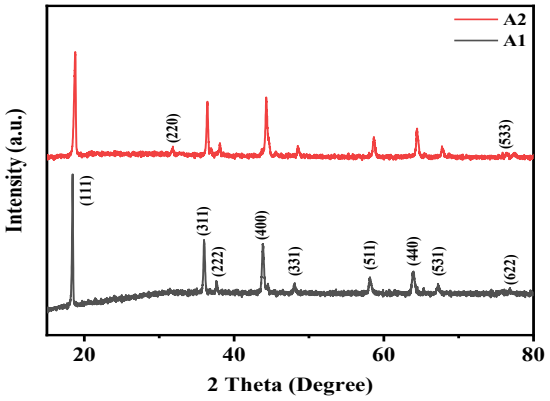

Figure 2: XRD pattern of the samples: A1) $LiMn_2O_4$, A2) $Li_{1.2}Mn_{1.6}Ni_{0.2}O_4$.

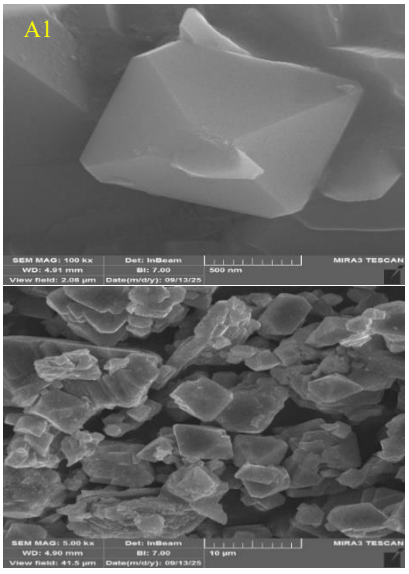

Figure 3: FE-SEM images of the samples A1) $LiMn_4O_2$.

Table 1: Some crystal parameters: A1) $LiMn_2O_4$, A2) $Li_{1.2}Mn_{1.6}Ni_{0.2}O_4$.

Sample	Average D (nm)	a (Å)	Lattice strain
A1	30.14	8.32	0.003
A2	28.94	8.19	0.003

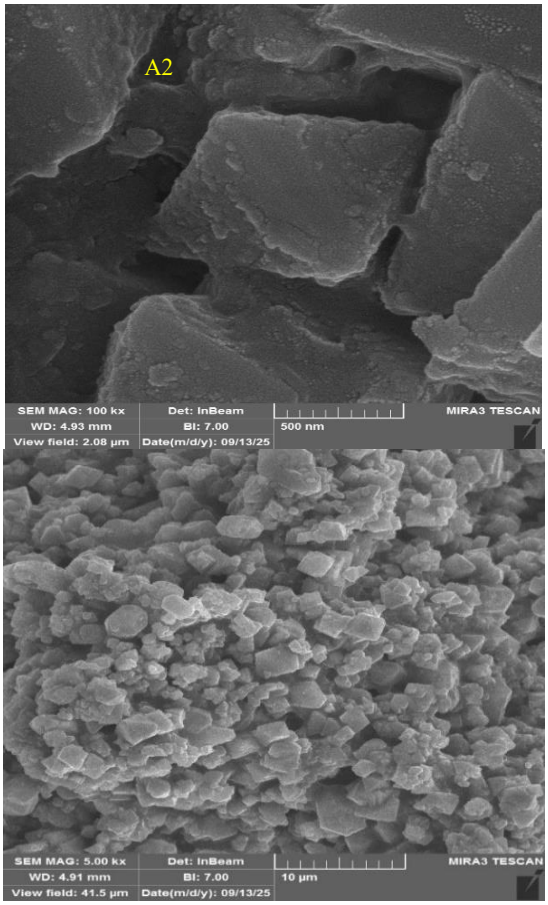

Figure 4: FE-SEM images of the samples A2) $Li_{1.2}Mn_{1.6}Ni_{0.2}O_4$.

Table 2: The ratio of chemical components in the samples A1) $LiMn_2O_4$, A2) $Li_{1.2}Mn_{1.6}Ni_{0.2}O_4$.

Samples	Element	Weight (%)	Atomic (%)
A1	O	32.52	62.33
	Mn	67.48	37.67
	Total	100	100
A2	O	38.2	68.18
	Mn	52.67	27.38
	Ni	9.13	4.44
	Total	100	100

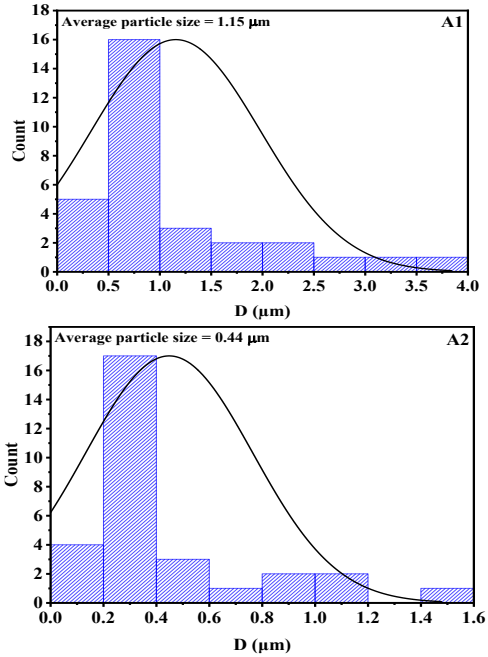

Figure 5: Distributions of particle sizes for the samples: A1) $LiMn_2O_4$, A2) $Li_{1.2}Mn_{1.6}Ni_{0.2}O_4$.

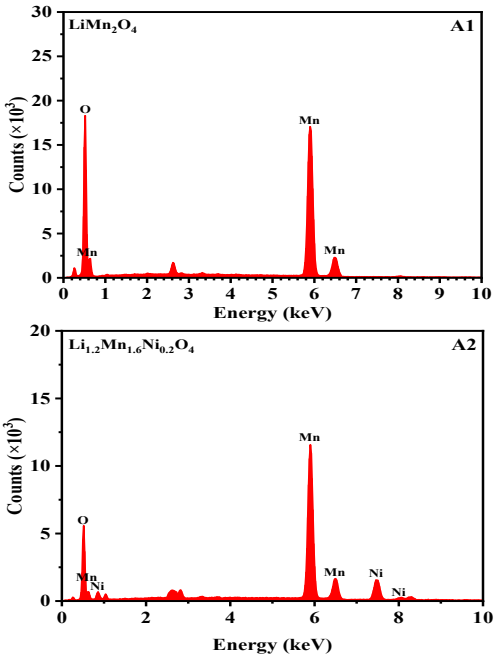

Figure 6: EDS examination of the samples: A1) $LiMn_2O_4$, A2) $Li_{1.2}Mn_{1.6}Ni_{0.2}O_4$.

3.4 Electrochemical Properties

3.4.1 Cyclic Voltammetry

Figure 7 shows the (CV) curves of $LiMn_2O_4$ and $Li_{1.2}Mn_{1.6}Ni_{0.2}O_4$ cathodes within the voltage range of (2.0-4.8) V and a scan rate of 0.1 mV s^{-1}. In the $LiMn_2O_4$ cathode, as shown in figure 7(A1), (CV) shows three oxidation/reduction peaks at potentials of (3.27/3.00) V, (3.73/3.47) V, and (4.56/4.27) V. These peaks are attributed to oxidation/reduction reactions between $Mn^{3+/}Mn^{3+}$ ions, associated with the insertion/extraction of lithium ions into and from the cathode [24], [25]. We note that there is a relatively large potential difference between the oxidation/reduction peaks, with potential difference ΔV values ranging between (0.26-0.29) V, indicating the presence of electrochemical polarization and non-ideal kinetics of lithium-ion transport within the cathode. This behavior is mostly attributed to the presence of Mn^{3+} ions, which exhibit Jahn-Teller distortion behavior, as this leads to the generation of distortions in the Mn-O bonds and stresses in the crystal lattice [26]. The $Li_{1.2}Mn_{1.6}Ni_{0.2}O_4$ cathode at Figure 7(A2) shows two main pairs of oxidation/reduction peaks at (3.44/3.21) V and (4.32/4.08) V, while the. These peaks within the range of (3.0-3.3) V are attributed to oxidation/reduction transitions between $Mn^{3+/}Mn^{4+}$, while the peaks within the range of (4.1-4.3) V are attributed to oxidation/reduction reactions between Ni^{3+}/Ni^{4+} [27]. The addition of nickel in structure improves the kinetics of lithium-ion insertion/extraction in the cathode and reduces polarization, which is clearly demonstrated by the lower ΔV values [28]. It is noteworthy that the increased lithium content and the addition of nickel in $Li_{1.2}Mn_{1.6}Ni_{0.2}O_4$, compared to $LiMn_2O_4$, contributes to raising the oxidation state of manganese towards Mn^{4+}, thereby reducing the number of Mn^{3+} ions associated with Jahn–Teller deformation behavior. This decrease in Mn^{3+} contributes to reducing structural deformations and stresses in the lattice and improvement in charge transport kinetics [29], [30], which is consistent with the CV curves showing oxidation/reduction behavior and the decrease in ΔV.

3.4.2 Electrochemical Impedance Spectroscopy (EIS)

In Figure 8, the Nyquist plot of the $LiMn_2O_4$ and $Li_{1.2}Mn_{1.6}Ni_{0.2}O_4$ cathodes shown. Shows the $LiMn_2O_4$ cathode, the electrolyte resistance R_s (10.98 Ω) and the charge-transfer resistance R_{ct} (317.63 Ω). The elevated (R_{ct}) value indicates sluggish charge-transfer kinetics across the electrode/electrolyte interface; the $Li_{1.2}Mn_{1.6}Ni_{0.2}O_4$ cathode shows (R_s = 13.59 Ω), while (R_{ct}) decreases to (289.10 Ω) compared with the $LiMn_2O_4$ cathode. Despite the slight increase in (R_s) upon nickel addition and increased lithium content, the pronounced decrease in (Rct) indicates an improvement in charge-transfer kinetics and a reduction in polarization, in agreement with the CV measurements [31]-[33].

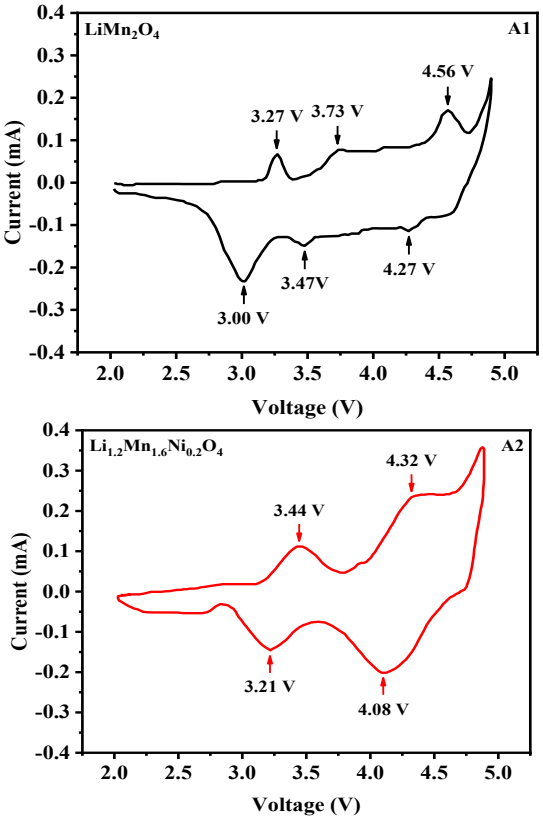

Figure 7: CV examination of the samples: A1) $LiMn_2O_4$, A2) $Li_{1.2}Mn_{1.6}Ni_{0.2}O_4$.

3.4.3 Galvanostatic Charge-Discharge (GCD)

Figure 9 (A1) shows the cathode $LiMn_2O_4$ which delivered a charge capacity of (213.45 mAh.g^{-1}) and a discharge capacity of (192.80 mAh.g^{-1}), corresponding to a coulombic efficiency of about (90.32%). The pronounced difference between the charge and discharge capacities reflects noticeable energy losses in the first cycle, which can be associated with high electrochemical polarization in addition to the limited mobility of lithium ions within the spinel structure of $LiMn_2O_4$. Figure 9(A2) shows that the

$Li_{1.2}Mn_{1.6}Ni_{0.2}O_4$ cathode exhibits a charge capacity of (245.82 $mAh.g^{-1}$) and a discharge capacity of (230.51 $mAh.g^{-1}$), with a coulombic efficiency of (93.77%). An improvement in capacity is evident, along with a reduced gap between the charge and discharge capacities, which indicates lower energy losses and a higher degree of efficient utilization of the active material during the lithium-ion insertion/extraction processes [34], [35].

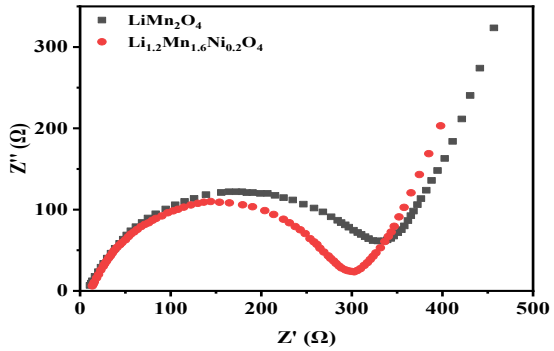

Figure 8: Nyquist plot of the $LiMn_2O_4$ and $Li_{1.2}Mn_{1.6}Ni_{0.2}O_4$.

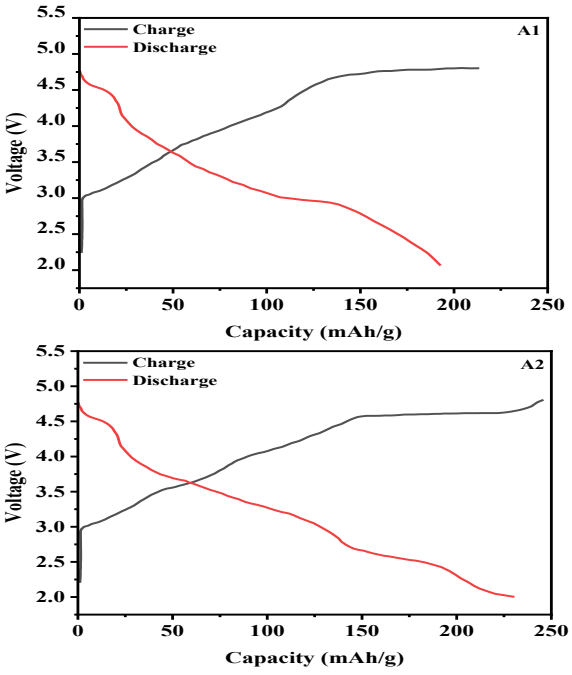

Figure 9: Charging - discharge curves: A1) $LiMn_2O_4$, A2) $Li_{1.2}Mn_{1.6}Ni_{0.2}O_4$.

3.4.4 Stability

Figure 10 illustrates the capacity retention as a function of the number of charge-discharge cycles for the cathodes $LiMn_2O_4$ and $Li_{1.2}Mn_{1.6}Ni_{0.2}O_4$ up to 100 cycles. The final capacity retention values after 100 cycles are listed in table 3, being (86.10%) for $LiMn_2O_4$ and (90.28%) for $Li_{1.2}Mn_{1.6}Ni_{0.2}O_4$. The undoped $LiMn_2O_4$ cathode exhibits a gradual decline in stability with increasing cycle number, with the capacity retention decreasing to (86.10%) after 100 cycles. This decrease reflects a limited structural stability under successive charge–discharge cycles and is consistent with the high (R_{ct}) values obtained from (EIS) measurements, in addition to the influence of Mn^{3+} ions associated with the Jahn-Teller distortion. These factors collectively lead to a progressive degradation of the spinel framework and a loss of a fraction of the non-recoverable capacity over repeated cycling. In contrast, the $Li_{1.2}Mn_{1.6}Ni_{0.2}O_4$ cathode shows improved stability, with the capacity retention increasing to approximately (90.28%) after 100 cycles. This enhancement indicates that introducing a moderate amount of (Ni) and increasing the Li content at the expense of Mn reinforce the structural stability of the crystal lattice and improve the kinetics of (Li^+) transport [36], [37].

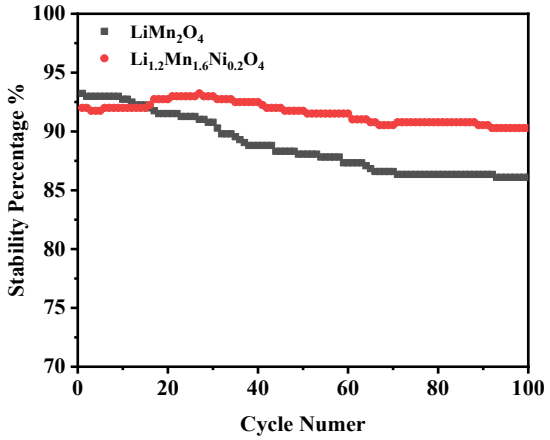

Figure 10: Nyquist plot of the $LiMn_2O_4$ and $Li_{1.2}Mn_{1.6}Ni_{0.2}O_4$.

Table 3: The stability percentage of samples: A1) $LiMn_2O_4$, A2) $Li_{1.2}Mn_{1.6}Ni_{0.2}O_4$.

Sample	Stability percentage
A1	86.10%
A2	90.28%

4 CONCLUSIONS

The results showed that employing a urea-assisted route followed by a two-step calcination process (450 °C for 4 h and then 800 °C for 5 h) is an effective strategy for synthesizing highly crystalline nanostructured spinel $LiMn_2O_4$ and $Li_{1.2}Mn_{1.6}Ni_{0.2}O_4$ powders. A pure spinel phase was obtained with a contraction of the lattice parameter from (8.32 to 8.19) Å and a reduction in the average crystallite size from (30.14 to 28.94) nm upon lithium enrichment and nickel doping, without compromising lattice stability. FE-SEM images revealed homogeneous octahedral morphologies for both materials, with a pronounced decrease in the average particle size from (1.15 to 0.44) μm for the doped sample, thereby enhancing the effective surface area and the diffusion pathways of lithium ions. From an electrochemical perspective, CV, EIS, and GCD measurements of coin-type lithium-ion cells fabricated and tested in this work demonstrated that the $Li_{1.2}Mn_{1.6}Ni_{0.2}O_4$ composition provides improved charge-transfer kinetics (a decrease in R_{ct} from 317.63 to 289.10 Ω) and lower polarization, along with higher initial charge/discharge capacities (245.82/230.51) $mAh \cdot g^{-1}$, higher coulombic efficiency (93.77%), and enhanced capacity retention after 100 cycles (90.28% compared with 86.10% for the undoped $LiMn_2O_4$ cathode). Accordingly, the prepared nanostructured cathodes, particularly $Li_{1.2}Mn_{1.6}Ni_{0.2}O_4$, demonstrate their practical efficiency in the high-voltage lithium-ion batteries assembled and evaluated in this study, while leaving scope for future work through exploring additional compositions, dopant levels, and more advanced operating conditions to meet the requirements of demanding industrial applications.

REFERENCES

[1] Y. Mahara et al., "Appearance of the 4 V signal without transformation to spinel-related oxides from loose-crystalline rock-salt LiMnO2," Journal of Power Sources, vol. 497, p. 229788, 2021.

[2] V. Etacheri, R. Marom, R. Elazari, G. Salitra, and D. Aurbach, "Challenges in the development of advanced Li-ion batteries: a review," Energy & Environmental Science, vol. 4, no. 9, pp. 3243-3262, 2011.

[3] N. Nasajpour-Esfahani et al., "Comprehensive review of lithium-ion battery materials and development challenges," Renewable and Sustainable Energy Reviews, vol. 203, p. 114783, 2024.

[4] G. G. Njema, R. B. O. Ouma, and J. K. Kibet, "A review on the recent advances in battery development and energy storage technologies," Journal of Renewable Energy, vol. 2024, no. 1, p. 2329261, 2024.

[5] X. Liu et al., "Advancements in Energy-Storage Technologies: A Review of Current Developments and Applications," Sustainability, vol. 17, no. 18, p. 8316, 2025.

[6] L. Quispe et al., "Synthesis of spinel LiNi0.5Mn1.5O4 by a wet chemical method and characterization for lithium-ion secondary batteries," Journal of the Ceramic Society of Japan, vol. 123, no. 1433, pp. 38-42, 2015.

[7] J. Ma, T. Liu, J. Ma, C. Zhang, and J. Yang, "Progress, Challenge, and Prospect of LiMnO2: An Adventure toward High-Energy and Low-Cost Li-Ion Batteries," Advanced Science, vol. 11, no. 2, p. 2304938, 2024.

[8] T. Zhao et al., "Oxidation Mechanism and Performance Control of Manganese-Based Catalysts in Soot Oxidation," Green Energy & Environment, 2024.

[9] Y. Miyaoka et al., "A Practical and Sustainable Ni/Co-Free High-Energy Electrode Material: Nanostructured LiMnO2," ACS Central Science, vol. 10, no. 9, pp. 1718-1732, 2024.

[10] M. Lazarraga et al., "Nanosize LiNiyMn2-yO4 (0< y≤ 0.5) spinels synthesized by a sucrose-aided combustion method. Characterization and electrochemical performance," Journal of Materials Chemistry, vol. 14, no. 10, pp. 1640-1647, 2004.

[11] K. M. Shaju and P. G. Bruce, "Nano-LiNi0.5Mn1.5O4 spinel: a high power electrode for Li-ion batteries," Dalton Transactions, no. 40, pp. 5471-5475, 2008.

[12] J. Zheng, P. Yan, L. Estevez, C. Wang, and J.-G. Zhang, "Effect of calcination temperature on the electrochemical properties of nickel-rich LiNi0.76Mn0.14Co0.10O2 cathodes for lithium-ion batteries," Nano Energy, vol. 49, pp. 538-548, 2018.

[13] Y. Han et al., "Preparation of layered Ni-rich LiNi0.9Co0.05Mn0.05O2 cathode materials with excellent electrochemical properties by controllable lithium supply and sintering," Journal of Energy Storage, vol. 67, p. 107541, 2023.

[14] J. K. Verma et al., "Impact of Ni Substitution on the Structural, Optical and Electronic Behavior of La2CrMnO6 Double Perovskite for Energy Applications," Open Journal of Composite Materials, vol. 15, no. 2, pp. 95-108, 2025.

[15] J. Wang et al., "Doping strategy in nickel-rich layered oxide cathode for lithium-ion battery," Renewables, vol. 1, no. 3, pp. 316-340, 2023.

[16] S. Young, Y. Chen, H. Chen, L. Horng, and J. Hsueh, "Effect of the substitutions of Ni3+, Co3+, and Fe3+ for Mn3+ on the ferromagnetic states of the La0.7Pb0.3MnO3 manganite," Journal of Applied Physics, vol. 91, no. 10, pp. 8915-8917, 2002.

[17] W. Ren, R. Luo, Z.-s. Liu, X.-y. Tan, Z.-y. Fu, and S.-j. Liao, "Effect of Ni/Mn ratio on the performance of LiNixMn2-xO4 cathode material for lithium-ion battery," Ionics, vol. 20, no. 10, pp. 1361-1366, 2014.

[18] K. Ariyoshi, H. Yamamoto, and Y. Yamada, "Relationship between changes in ionic radius and lattice dimension of lithium manganese oxide spinels during lithium insertion/extraction," Solid State Ionics, vol. 343, p. 115077, 2019.

[19] N. Hassan and M. Al-Timimi, "Structural and electrochemical properties of LiMn1-xCrxO2 cathode for enhanced lithium-ion battery," Journal of Ovonic Research, vol. 21, no. 1, 2025.

[20] S. Liu, Q. Huo, R. Chen, P. Chen, Y. Li, and Y. Han, "Synthesis and characterization of an iron nitride constructed by a novel template of metal organic framework," Journal of Spectroscopy, vol. 2015, no. 1, p. 362103, 2015.

[21] S. Yoon, "Effect of nitridation on LiMn1.5Ni0.5O4 and its application as cathode material in lithium-ion batteries," Journal of Applied Electrochemistry, vol. 46, no. 4, pp. 479-485, 2016.

[22] K. Prakasha and A. Prakash, "A time and energy conserving solution combustion synthesis of nano Li1.2Ni0.13Mn0.54Co0.13O2 cathode material and its performance in Li-ion batteries," RSC Advances, vol. 5, no. 114, pp. 94411-94417, 2015.

[23] N. M. Ali, M. Al-TIMIMI, O. A. A.-J. Al-Jubouri, H. T. Homad, and E. J. Lavasani, "Hydrothermal Method for Synthesizing and Characterizing LiMn2O4 as a Cathode Material for Rechargeable (Li-ion) Battery Applications," Academic Science Journal, vol. 3, no. 2, pp. 254-274, 2025.

[24] Y. Hou, K. Chang, H. Tang, B. Li, Y. Hou, and Z. Chang, "Drastic enhancement in the rate and cyclic behavior of LiMn2O4 electrodes at elevated temperatures by phosphorus doping," Electrochimica Acta, vol. 319, pp. 587-595, 2019.

[25] J. Ma et al., "Si-Al co-doping synergistically enhances the high-rate capacity and long-cycle life of spinel LiMn2O4," Journal of Power Sources, vol. 646, p. 237218, 2025.

[26] B. Li et al., "Strengthening reversibility at high rate of spinel LiMn2O4 by aluminum and copper co-doping for lithium ion battery," Electrochimica Acta, vol. 464, p. 142898, 2023.

[27] H. Ding et al., "Improving electrochemical performances of LiNi0.5Mn1.5O4 by the strategy of oxygen vacancy doping," Applied Materials Today, vol. 38, p. 102248, 2024.

[28] L. Huang and Y. Wu, "Spinel Ni-doped LiMn2O4 cathode material with high oxygen reduction catalytic performance for low temperature solid ceramic fuel cells," Ceramics International, vol. 50, no. 3, pp. 5150-5159, 2024.

[29] W. Xu et al., "Unveiling the role of Ni doping in the electrochemical performance improvement of the LiMn2O4 cathodes," Applied Surface Science, vol. 624, p. 157142, 2023.

[30] L. Chen et al., "A general molten salt method to conduct doping engineering for high-performance LiMn2O4 cathode," Journal of Energy Storage, vol. 102, p. 114217, 2024.

[31] J. K. Yadav, P. Saini, B. Rani, and A. Dixit, "Al2O3@LiMn2O4 nanoparticles cathodes for high-rate Li-ion batteries," Materials Letters, vol. 387, p. 138265, 2025.

[32] Y.-S. Hsiao et al., "Designing core-shell LiNi0.5Mn1.5O4-based cathode materials with enhanced rate capability and improved cycling stability," Applied Surface Science, vol. 684, p. 161892, 2025.

[33] A. Iqbal, Y. Iqbal, A. M. Khan, and S. Ahmed, "Effect of bication (Cu-Cr) substitution on the structure and electrochemical performance of LiMn2O4 spinel cathodes at low and high current rates," Journal of Saudi Chemical Society, vol. 22, no. 4, pp. 449-458, 2018.

[34] M. Hashem, S. M. Abbas, X. Hou, A. E. Eid, and A. E. Abdel-Ghany, "Facile one step synthesis method of spinel LiMn2O4 cathode material for lithium batteries," Heliyon, vol. 5, no. 7, 2019.

[35] T. Zhao et al., "Three-dimensional Li1.2Ni0.2Mn0.6O2 cathode materials synthesized by a novel hydrothermal method for lithium-ion batteries," Journal of Alloys and Compounds, vol. 757, pp. 16-23, 2018.

[36] Y. Pan, Y. Li, L. Hu, Y. Yang, J. Guo, and S. Yang, "Enhancing the cycling stability of spinel LiMn2O4 via Ni-Co surface gradient doping: Mechanisms of structural stabilization and Mn dissolution mitigation," Journal of Power Sources, vol. 650, p. 237527, 2025.

[37] Y. Ji et al., "Improved capacity retention and ultralong cycle performance of Ni-Fe co-doped LiMn2O4 cathode material at high current densities," Colloids and Surfaces A: Physicochemical and Engineering Aspects, vol. 648, p. 129259, 2022.